Research Article | Vol. 25, No. 25 | 11 Dec 2017 | OPTICS EXPRESS 30843
Optics EXPRESS

Ultraviolet photodetector using pn junction formed by transferrable hollow n-TiO_2 nano-spheres monolayer

TAEYOUNG YANG,[1,3] SEONG-JIN PARK,[2,3] TAEK GON KIM,[1] DONG SU SHIN,[1] KYUNG-DO SUH,[2] AND JINSUB PARK[1,*]

[1]*Department of Electronics and Computer Engineering, Hanyang University, Seoul 04763, South Korea*
[2]*Department of Chemical Engineering, Hanyang University, Seoul 04763, South Korea*
[3]*Authors contributed equally this work.*
[*]*jinsubpark@hanyang.ac.kr*

Abstract: We report an ultraviolet (UV) photodetector with a universally transferable monolayer film with ordered hollow TiO_2 spheres on p-GaN. After forming a TiO_2 monolayer film by unidirectional rubbing of hollow TiO_2 spheres on a polydimethylsiloxane (PDMS) supporting plate, we used a 5% polyvinyl alcohol (PVA) aqueous solution to transfer the film onto the target substrate. The PVA/TiO_2 monolayer film was detached from the PDMS film and transferred to the p-GaN/Al_2O_3 substrate. To investigate the effects of crystallized phases of the TiO_2 hollow spheres, anatase and rutile TiO_2 sphere monolayers prepared by combining template synthesis and thermal treatment. The responsiveness of the UV photodetectors using anatase and rutile hollow n-TiO_2 monolayer/p-GaN was 0.203 A/W at 312 nm and 0.093 A/W at 327 nm, respectively.

OCIS codes: (040.0040) Detectors; (250.0250) Optoelectronics; (040.5160) Photodetectors; (040.7190) Ultraviolet.

References and links

1. W. C. Tsai, H. L. Kao, K. H. Liao, Y. H. Liu, T. P. Lin, and E. S. Jeng, "Room temperature fabrication of ZnO/ST-cut quartz SAW UV photodetector with small temperature coefficient," Opt. Express **23**(3), 2187–2195 (2015).
2. M. Zhang, H. Zhang, K. Lv, W. Chen, J. Zhou, L. Shen, and S. Ruan, "Ultraviolet photodetector with high internal gain enhanced by TiO_2/$SrTiO_3$ heterojunction," Opt. Express **20**(6), 5936–5941 (2012).
3. E. Monroy, F. Vigue, F. Calle, J. I. Izpura, E. Munoz, and J. P. Faurie, "Time response analysis of ZnSe-based Schottky barrier photodetectors," Appl. Phys. Lett. **77**(17), 2761–2763 (2000).
4. R. C. Jayasinghe, A. G. Perera, H. Zhu, and Y. Zhao, "Optical properties of nanostructured TiO2 thin films and their application as antireflection coatings on infrared detectors," Opt. Lett. **37**(20), 4302–4304 (2012).
5. B. Park, H. Im, and S. J. Woo, "Resistive Switching Properties of a Polycrystalline TiO_2 Memory Cell with a Tungsten Nitride (WN) Bu er Layer Inserted," J. Korean Phys. Soc. **53**(6), 3685–3689 (2008).
6. A. M. Selman, Z. Hassan, M. Husham, and N. M. Ahmed, "A high-sensitivity, fast-response, rapid-recovery p-n heterojunction photodiode based on rutile TiO_2 nanorod array on p-Si (111)," Appl. Surf. Sci. **35**, 445–452 (2014).
7. U. M. Nayef, K. A. Jubeatir, and Z. J. Abdulkareem, "Ultraviolet photodetector based on TiO_2 nanoparticles/porous silicon heterojunction," Optik (Stuttg.) **127**, 2806–2810 (2016).
8. A. M. Z. Hassan, "Highly sensitive fast-response UV photodiode fabricated from rutile TiO_2 nanorod array on silicon substrate," Sens. Actuators A Phys. **221**, 15–21 (2015).
9. H. Yin, Y. Wada, T. Kitamura, S. Kambe, S. Murasawa, H. Mori, T. Sakata, and S. Yanagida, "Hydrothermal synthesis of nanosized anatase and rutile TiO_2 using amorphous phase TiO_2," J. Mater. Chem. **11**(6), 1694–1703 (2001).
10. S. Agarwala, M. Kevin, A. S. W. Wong, C. K. N. Peh, V. Thavasi, and G. W. Ho, "Mesophase ordering of TiO_2 film with high surface area and strong light harvesting for dye-sensitized solar cell," ACS Appl. Mater. Interfaces **2**(7), 1844–1850 (2010).
11. N. Arconada, A. Durán, S. Suárez, R. Portela, J. M. Coronado, B. Sánchez, and Y. Castro, "Synthesis and photocatalytic properties of dense and porous TiO_2-anatase thin films prepared by sol–gel," Appl. Catal. B **86**(1), 1–7 (2009).
12. G. K. Goh, S. K. Donthu, and P. K. Pallathadka, "Cracking and orientation of solution-deposited rutile TiO_2 films," Chem. Mater. **16**(15), 2857–2861 (2004).
13. C. Park, T. Lee, Y. Xia, T. J. Shin, J. Myoung, and U. Jeong, "Quick, Large-Area Assembly of a Single-Crystal Monolayer of Spherical Particles by Unidirectional Rubbing," Adv. Mater. **26**(27), 4633–4638 (2014).

#307164 https://doi.org/10.1364/OE.25.030843
Journal © 2017 Received 14 Sep 2017; revised 8 Nov 2017; accepted 8 Nov 2017; published 27 Nov 2017

Optics EXPRESS

14. H. E. Wang, L. X. Zheng, C. P. Liu, Y. K. Liu, C. Y. Luan, H. Cheng, and I. Bello, "Rapid microwave synthesis of porous TiO_2 spheres and their applications in dye-sensitized solar cells," J. Phys. Chem. C **115**(21), 10419–10425 (2011).
15. K. A. Kwon, H. S. Lim, Y. K. Sun, and K. D. Suh, "α-Fe_2O_3 submicron spheres with hollow and macroporous structures as high-performance anode materials for lithium ion batteries," J. Phys. Chem. C **118**(6), 2897–2907 (2014).
16. S. J. Park, H. S. Lim, Y. M. Lee, and K. D. Suh, "Facile synthesis of monodisperse poly (MAA/EGDMA)/Fe_3O_4 hydrogel microspheres with hollow structures for drug delivery systems: the hollow structure formation mechanism and effects of various metal ions on structural changes," RSC Advances **5**(13), 10081–10088 (2015).
17. K. F. Azizi and M. M. Bagheri-Mohagheghi, "Transition from anatase to rutile phase in titanium dioxide (TiO_2) nanoparticles synthesized by complexing sol–gel process: effect of kind of complexing agent and calcinating temperature," J. Sol-Gel Sci. Tech. **65**(3), 329–335 (2013).
18. H. C. Weerasinghe, P. M. Sirimanne, G. V. Franks, G. P. Simon, and Y. B. Cheng, "Low temperature chemically sintered nano-crystalline TiO_2 electrodes for flexible dye-sensitized solar cells," J. Photoch. Photobio. A **213**(1), 30–36 (2010).
19. W. Zhou, Y. Liu, Y. Zhang, G. Yang, S. Deng, F. Shen, and L. Wang, "Novel multi-layer cross-linked TiO_2/C nanosheets and their photocatalytic propertiesm," New J. Chem. **38**(4), 1647–1654 (2014).
20. H. S. Lim, J. Lee, S. Lee, Y. S. Kang, Y. K. Sun, and K. D. Suh, "Walnut-like ZnO@Zn_2TiO_4 multicore-shell submicron spheres with a thin carbon layer: Fine synthesis, facile structural control and solar light photocatalytic application," Acta Mater. **122**, 287–297 (2017).
21. F. T. Johra, J. W. Lee, and W. G. Jung, "Facile and safe graphene preparation on solution based platform," J. Ind. Eng. Chem. **20**(5), 2883–2887 (2014).
22. S. K. Park, J. S. Jeong, T. K. Yun, and J. Y. Bae, "Preparation of Carbon-Doped TiO_2 and Its Application as a Photoelectrodes in Dye-Sensitized Solar Cells," J. Nanosci. Nanotechnol. **15**(2), 1529–1532 (2015).
23. A. Slav, "Optical characterization of TiO_2-Ge nanocomposite films obtained by reactive magnetron sputtering," Dig. J. Nanomater. Biostruct. **6**(3), 915–920 (2011).
24. A. Amtout and R. Leonelli, "Optical properties of rutile near its fundamental band gap," Phys. Rev. B Condens. Matter **51**(11), 6842–6851 (1995).

1. Introduction

For ultraviolet (UV) detection, wide-band-gap semiconductors such as ZnO, SiC, ZnSe, and TiO_2 have been used for photoresponse wavelength matching between the bandgap and absorption of UV radiation [1–3]. Among the wide-band-gap compound semiconductors, TiO_2 has received a great deal of attention due to its high power-conversion efficiency, relative ease with which the structure can be controlled, low cost, and resistive switching properties, relative to other compound semiconductors [4,5]. In order to fabricate the UV photodetectors, the hetero pn junction using metal oxide nanostructures formed on various templates or substrates were attempted [6]. Recently, the UV photodetectors using TiO_2 nanorods and nanoparticles based heterojunction formed on p-Si substrates were reported [7,8]. Although TiO_2 thin films consisting of nanoparticles formed by a spin-coating process has been widely used for a wide range of applications due to its many advantages, the main drawback affecting its application to optoelectronic devices is the problem of surface cracks forming in the TiO_2 films [9,10]. After the formation of a TiO_2 thin film on a target substrate by a simple spin-coating method, a post-annealing process is essential to remove the binders and impurities which may be incorporated into the TiO_2 nanoparticles during the synthesis reaction in a solution-based process. During a heat-treatment process, tensile stress builds up in a TiO_2 thin film due to the shrinkage of the xerogel film. This adversely affects the stability of the TiO_2 film due to the easy formation of surface cracks [11]. The cracks that form in the TiO_2 films of a pn-junction-based device can act as leakage current paths in operation mode, resulting in the degradation of the optoelectronic device performance, including the optical and electrical characteristics.

In this study, we fabricated UV photodetectors using a transferable n-TiO_2 monolayer film/p-GaN based pn junction structure. The formation of the ordered TiO_2 thin film with nano-sized hollow TiO_2 spheres and its transfer onto the target substrate were achieved by a simple unidirectional rubbing method and a PVA supporting film [12]. The control and the effects of the crystal phases of TiO_2 hollow spheres on the performance of UV detectors were investigated using current-voltage (I-V) probing and photo-responsiveness. Our suggested transferrable n-TiO_2 hollow spheres monolayer/p-GaN pn junction structure has great

Optics EXPRESS

potential for application to a wide range of optoelectronic devices including UV photodetectors.

2. Experimental details

A transferable hollow TiO_2 nanosphere monolayer was used for an n-type film placed on a p-GaN template to fabricate a pn junction for application to UV detectors. Hollow nanostructures can effectively increase the light-scattering effect in an inner free space covered by a shell layer, resulting in the enhancement of the photo-responsiveness of a UV detector [13]. To form hollow TiO_2 spheres, a template method was used as described in the literature [14]. The sacrificial template, used to make the hollow TiO_2 spheres, consisted of poly(MAA/EGDMA) microspheres that were synthesized by a distillation precipitation polymerization process [15]. To maintain the size of the final hollow TiO_2 spheres at about 350 nm, poly(MAA/EGDMA) microspheres with 610-nm-diameter were used. Methacrylic acid (MAA, 14 g) and ethyleneglycol dimethacrylate (EGDMA, 6 g) were polymerized at 88 °C for 150 min in a medium consisting of acetonitrile (AN) and deionized (DI) water, as well as α, α'-azobis (isobutyronitrile) (AIBN). EGDMA and AIBN were used as a cross-linker and initiator, respectively [16]. After polymerization, the remaining residues were removed and purified by centrifugation with ethanol and DI water. The TiO_2 shell layer was formed over the poly(MAA/EGDMA) microspheres by a formation reaction conducted in a 1-L four-neck glass reactor with a stirring bar using titanium isopropoxide (TTIP) as the TiO_2 precursor. We dispersed 2 g of each of the poly(MAA/EGDMA) microspheres into 200 mL of ethanol in a reactor for 2 h. A mixture, consisting of 1.4 g of TTIP and 100 mL of ethanol, was poured into the glass reactor. The solution was then stirred in the reactor for 24 h and then centrifuged at 3600 rpm for 10 min to filter out the residues. The final products were then dried in a vacuum oven. The as-prepared core/shell poly(MAA/EGDMA)/amorphous TiO_2 microspheres were annealed at 450 °C and 700 °C for 4 h to control the crystallized phases of, respectively, the anatase and rutile TiO_2 submicron spheres with hollow structures.

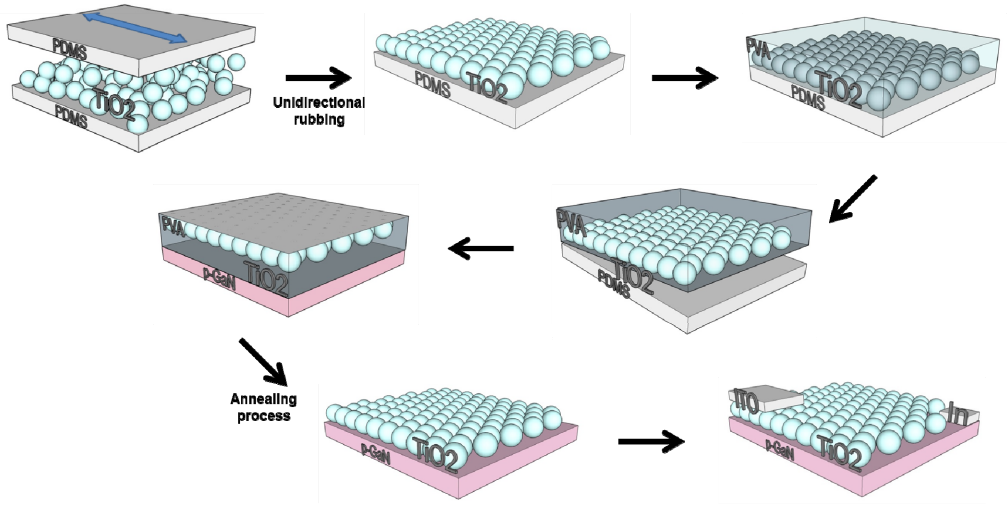

Fig. 1. Fabrication of UV photodetector using n-TiO_2 monolayer/p-GaN junction.

Figure 1 is a schematic diagram of the pn junction formation process using a transferable TiO_2 monolayer and a p-GaN template. To make TiO_2 monolayers using hollow TiO_2 spheres, we applied the unidirectional rubbing method as described in the literature [12]. First, two flat polydimethylsiloxane (PDMS) flexible plates were formed in a petri dish. Then a film of hollow TiO_2 spheres was supported on one of the PDMS plates and rubbed with the other PDMS supporting plate. After sufficient rubbing, the extra TiO_2 nanospheres were

Optics EXPRESS

pushed to the edge of the PDMS plate and were then removed by blowing with N_2 gas. Then, 3 g of 5% polyvinyl alcohol (PVA) solution was poured onto the TiO_2 monolayer/PDMS supporting plate to form a PVA/TiO_2 monolayer/PDMS film. The 5% PVA solution spread uniformly to create a PVA/TiO_2 monolayer film after aging for 24 h under a vacuum. After the formation of the TiO_2 monolayer film, covered with PVA, the PVA/TiO_2 monolayer film was peeled from the PDMS supporting plate. The detached PVA/TiO_2 monolayer films were then transferred onto p-GaN/Al_2O_3 substrates to fabricate pn junction-based UV photodetectors. The TiO_2 monolayer/PVA/p-GaN structures were heated to 450°C for 4 h to evaporate the PVA film. After the transfer of the ordered-monolayer of hollow TiO_2 spheres onto the p-GaN, an indium electrode was deposited onto the p-GaN and a 100-nm ITO film, formed on glass, was used as the electrode for the n-TiO_2 monolayer.

The I-V characteristics of the n-TiO_2 monolayer/p-GaN junction structures were examined using a Keithley 2400 source meter and a UV lamp. Photo-responsivity measurements with respect to a change in the wavelength were carried out using a K3100 incident photon conversion efficiency (IPCE) measurement system.

3. Results and discussion

To investigate the effects of the crystal phase of the TiO_2 on the device performance, we modified the crystal phase of the as-synthesized amorphous hollow TiO_2 spheres to the anatase and rutile phases by changing the post-annealing process conditions. To confirm the phase change of the TiO_2 spheres after annealing at different temperatures, we observed the XRD patterns. Figures 2(a)-2(c) show the XRD spectra of the as-synthesized, anatase-, and rutile-phase hollow TiO_2 spheres deposited on quartz glass. For the as-synthesized core/shell TiO_2/poly(MAA/EGDMA) spheres, there are no strong peaks in the XRD pattern, indicating that there is no crystallized phase, as shown in Fig. 2(a). By increasing the annealing temperature to 450 °C for 4 h, 2θ peaks appeared at 25.281°, 48.049°, and 55.060°, as shown in Fig. 2(b). These dominant XRD peaks are in good agreement with the (101), (200), and (211) plane peaks of the anatase-structured TiO_2 crystal (JCPDS no. 21-1272). Moreover, after annealing the as-synthesized TiO_2 at 700 °C, the XRD peaks mainly exhibited (110), (211), and (101) plane-related peaks at 2θ = 27.446°, 54.322°, and 36.085°, respectively, as shown in Fig. 2(c). This is in good agreement with the rutile-structured TiO_2 crystal (JCPDS no. 21-1276). According to the JCPDS references, as-synthesized amorphous TiO_2 spheres change to anatase- and rutile-phase TiO_2 as a result of heat treatment performed at 450 °C and 700 °C, respectively [17]. In addition, no poly(MAA/EGDMA) peaks were observed in the XRD patterns of either the anatase or rutile TiO_2 due to the removal of the carbon, hydrogen, and oxygen content. The carbon and hydrogen components of the organic materials combined with O_2 during annealing in an air atmosphere such that the carbon and hydrogen were removed.

The surface morphology and size of the core/shell structures of the TiO_2/poly(MAA/EGDMA) spheres, both before and after the thermal annealing process, were evaluated by SEM measurements. Figure 3 shows the as-synthesized TiO_2/poly(MAA/EGDMA) spheres, as well as the hollow anatase and rutile TiO_2 spheres after annealing at 450 °C and 700 °C for 4 h, respectively. The hollow structure is well retained after the annealing process due to the interconnection of the TiO_2 nanoparticles [18]. The size of the core/shell TiO_2/poly(MAA/EGDMA) decreased from about 610 nm to 360 and 335 nm after the formation of the anatase and rutile hollow TiO_2 spheres, as a result of the shrinkage of the core/shell structures by thermal annealing. The higher-temperature annealing process used to attain rutile hollow TiO_2 structures causes the hollow TiO_2 spheres to be broken into small pieces.

Optics EXPRESS

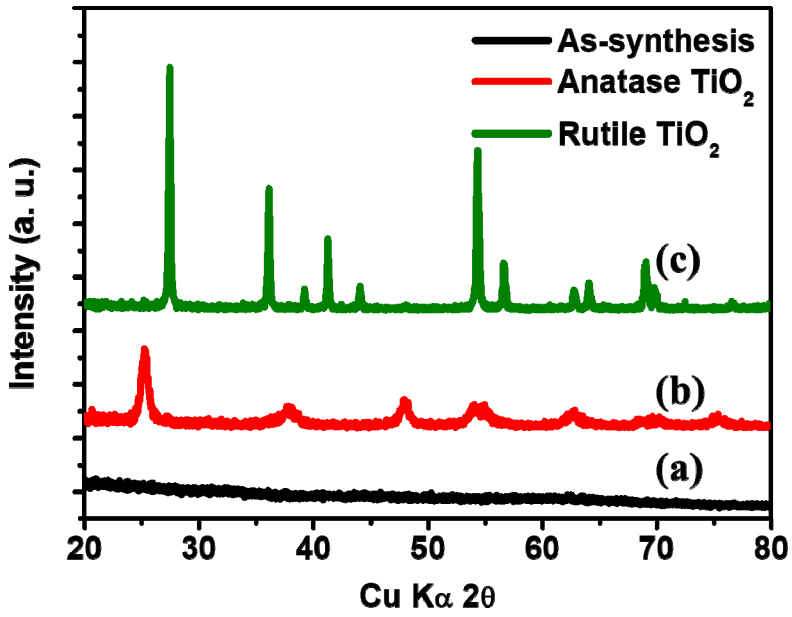

Fig. 2. XRD spectra obtained from TiO_2 spheres with (a) as-synthesized, (b) anatase, and (c) rutile structure.

To fabricate a well-arranged TiO_2 thin film, after transfer of TiO_2 monolayer film covered with PVA solution to enable transfer to a targeted substrate, the PVA was solidified by the application of a small amount of heat, after which the PVA/TiO_2 monolayer film could be transferred to the p-GaN. The second annealing process is necessary to remove the PVA. SEM images were obtained for the TiO_2 monolayer films with anatase and rutile hollow TiO_2 spheres, as shown in Figs. 3(d) and 3(e), respectively. After the second annealing process in air, the PVA was removed by the reaction between the carbon in the PVA and oxygen in the air.

During the second annealing process, the outer TiO_2 spheres melted slightly and became connected to other spheres. These slightly melted TiO_2 structures with carbon residue between the TiO_2 spheres produce a strong connection with the other spheres. The electrical conductivity through the carbon-wrapped TiO_2 monolayer was improved by reducing the number of disconnections and maintaining the special distance between the TiO_2 spheres [19].

From the EDS results (not shown here), we observed that some carbon residue remained after the burning of the PVA during the annealing process in an air atmosphere. To better understand the carbon residue originating from the PVA after the second annealing process, the surface chemistry was examined by using XPS, as shown in Figs. 4(a) and 4(b). The C 1s spectrum consists of four peaks. For the anatase TiO_2 monolayer shown in Fig. 4(c), the peaks located at 284.38, 284.98, and 288.08 eV were attributed to the C-C, C-O, and C = O bonds, respectively. Furthermore, in the case of the rutile TiO_2 monolayer shown in Fig. 4(d), the peaks located at 284.53, 285.98, and 288.58 eV were assigned to the C-C, C-O, and C = O bonds, respectively. These results are acceptable when compared with previously reported values [18,20]. Among three carbon bonds (C-C, C-O, and C = O), C-C bonding contributes to the enhanced electrical conductivity of carbon [21]. Figures 4(a) and 4(b) show that C-C bonding is dominant in the TiO_2 monolayer, while the peak intensity of the oxidized carbon was relatively low, which can lead to a decrease in the electrical conductivity.

Optics EXPRESS

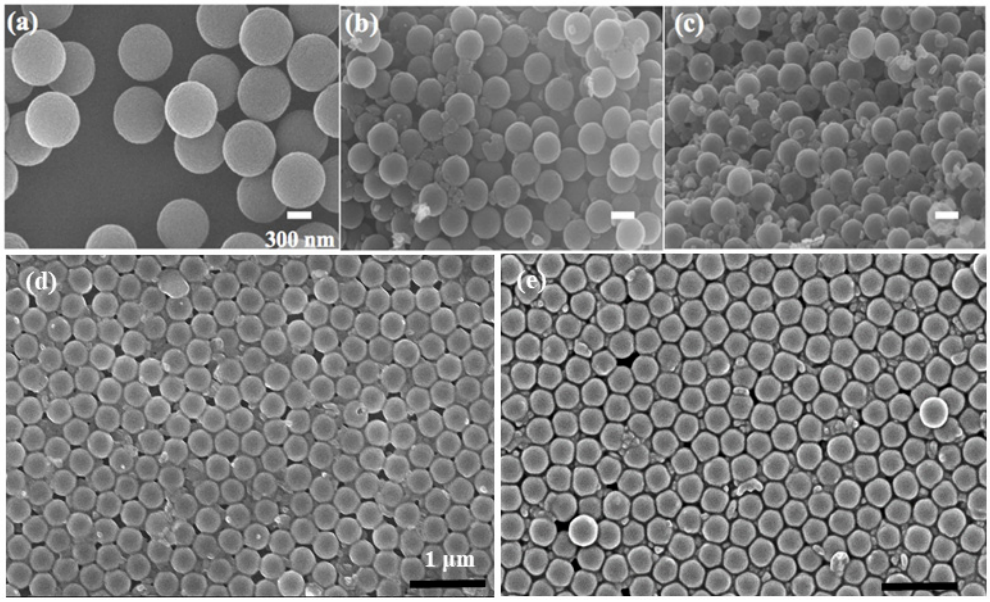

Fig. 3. SEM images of poly(MAA/EGDMA)/α-TiO_2 particles (a) before annealing process, after annealing process at (b) 450 °C and (c) 700 °C in air atmosphere. TiO_2 monolayer transferred onto p-GaN template using (d) anatase TiO_2 spheres (e) rutile TiO_2 spheres.

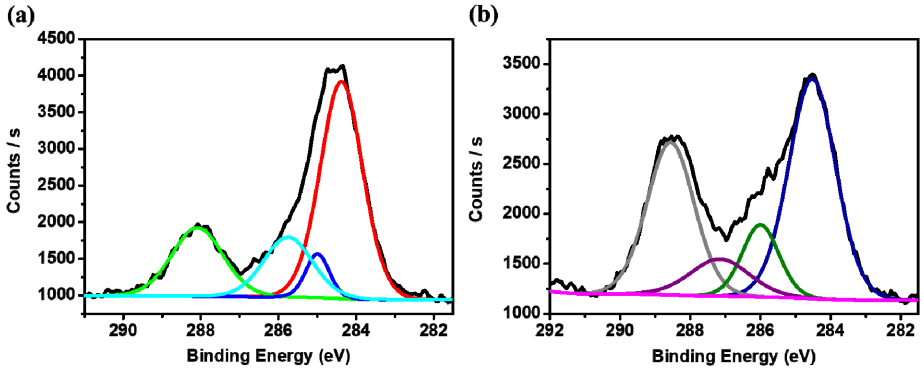

Fig. 4. XPS spectrum (C 1s) of TiO_2 monolayer using (a) anatase and (b) rutile TiO_2 spheres.

Therefore, TiO_2 spheres connected by carbon (C-C) exhibit a better electrical conductivity than pure TiO_2. Therefore, the carbon residues influence the electrical properties of the hollow TiO_2 spheres and the performance of UV photodetectors due to the superior conductivity of n-TiO_2 monolayers [22].

To investigate the optical properties of the anatase and rutile TiO_2 monolayers, the absorbance was measured by applying UV-VIS spectroscopy. Figure 5(a) shows the absorbance spectra of the anatase (red line) and rutile (green line) TiO_2 monolayers. It clearly shows that the anatase and rutile TiO_2 monolayers absorb only UV light due to their wide band gap. We calculated the optical band gap of the TiO_2 monolayers and p-GaN from a Tauc plot, shown in Fig. 5(b), as a plot of the $(ahv)^{1/2}$ versus hv curves [23].

$$ahv = A(hv - E_g)^{m}$$

Optics EXPRESS

Here, A is a constant, hv is the incident photon energy, E_g is the optical band gap, α is an absorption coefficient, and the value of m is 2 for indirect transitions. The calculated band gaps for the anatase and rutile TiO_2 monolayer are about 3.27, and 2.95 eV, respectively [24].

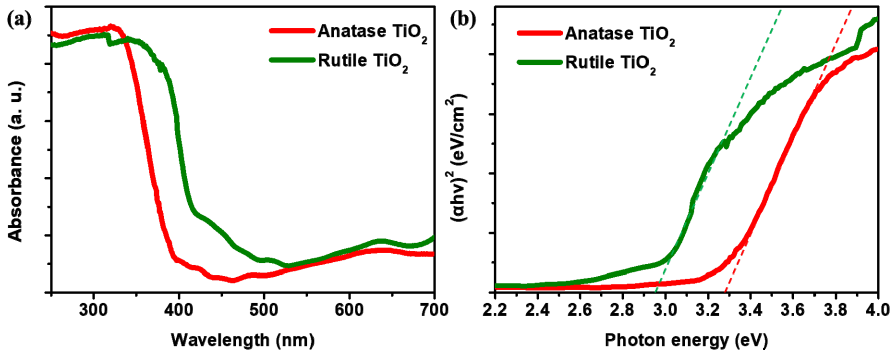

Fig. 5. (a) Absorbance spectra of TiO_2 monolayers using anatase and rutile TiO_2 spheres. (b) Tauc plot for band gap calculation of TiO_2 monolayer with different phases.

The electrical properties of the anatase- and rutile-structured n-TiO_2 monolayer/p-GaN junctions were measured by using an I-V probing system under both UV light illumination and darkness. Figures 6(a) and 6(b) show the good rectifying behavior of both anatase and rutile TiO_2 monolayer junction structures under reverse-bias conditions. The reverse currents of the anatase- and rutile-structured TiO_2 monolayer were −0.58 μA and −0.029 μA, respectively, at −8.8 V under the no-light condition. After illuminating the pn junction structures with UV light, the reverse currents for the anatase and rutile TiO_2 monolayer structures were increased to −4.29 μA and −0.44 μA, respectively, at −8.8 V. The increased absolute current of the anatase TiO_2 monolayer/p-GaN junction was 3.71 μA upon the change from the dark state to UV illumination, which was higher than that of the rutile TiO_2 monolayer junction (0.411 μA). The pn junction consisting of the transferred n-TiO_2 monolayer film onto the p-GaN template effectively generated electron-hole pairs (EHPs) under UV light, which may be the source of the additional current flow through the pn junction under reverse-bias conditions. Moreover, the anatase TiO_2 monolayer/p-GaN structure provides a more efficient means of generating excess carriers under UV illumination than a pn junction based on a rutile TiO_2 monolayer. The performances of n-TiO_2 monolayers/p-GaN photodetectors consisting of anatase and rutile phases were evaluated in terms of their photo-responsiveness by applying a spectral IPCE measurement system. As shown in Fig. 6(c), the peak responsivity of the anatase- and rutile-structured TiO_2 monolayer/p-GaN pn junctions are 0.203 A/W at 312 nm and 0.093 A/W at 327 nm. The responsivity of a pn junction based on an anatase TiO_2 monolayer junction is better than that of a device based on a rutile TiO_2 monolayer. This phenomenon can be attributed to the different electron transport behaviors in the different phases of the TiO_2 hollow spheres. The effective diffusion coefficient of anatase TiO_2 is greater than that of rutile-structured TiO_2, meaning that the electron transport in anatase TiO_2 is easier than in rutile TiO_2. Another possible reason for the superior performance of a detector based on an anatase TiO_2 monolayer is related to the different effective masses of the electrons with respect to the phase change. Anatase-structured TiO_2 has a smaller electron effective mass as well as a longer recombination lifetime than rutile TiO_2. This means that additionally generated EHPs in anatase TiO_2 resulting from UV irradiation of the devices can survive longer with higher mobility than ones in rutile TiO_2 monolayer. Therefore, an anatase TiO_2 monolayer photodetector exhibits a photo-response performance that is superior to that of one based on a rutile-structured TiO_2 monolayer.

Optics EXPRESS

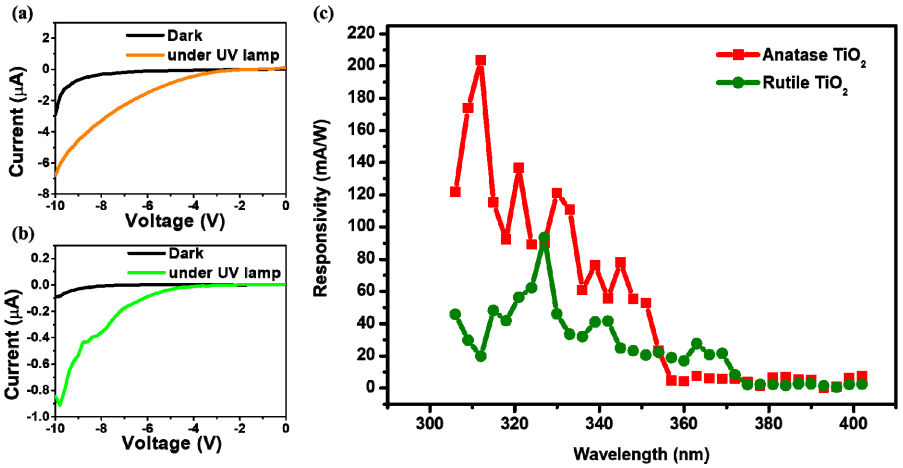

Fig. 6. I-V characteristics of TiO_2 monolayer/p-GaN pn junction using (a) anatase TiO_2 spheres (b) rutile TiO_2 spheres. (c) Responsiveness of TiO_2 monolayer/p-GaN pn junction using anatase and rutile TiO_2 spheres (−9 V bias).

4. Conclusions

In summary, we successfully transferred a n-TiO_2 monolayer consisting of hollow TiO_2 spheres onto p-GaN to form a pn junction to demonstrate the new TiO_2 film type and investigate its application to optoelectronic fields. The effects of the TiO_2 monolayer with different phases of sphere on the performance of a fabricated UV photodetector were investigated. The I-V characteristics of all the n-TiO_2 monolayer/p-GaN junctions exhibit good rectifying properties. To demonstrate the feasibility of our suggested structures for application to UV photodetectors, we compared the spectral responsiveness of anatase and rutile TiO_2 monolayer/p-GaN pn junctions. The anatase TiO_2 monolayer/p-GaN junction performed better as a UV photodetector than a pn junction based on a rutile TiO_2 monolayer due to the faster electron transport of the anatase TiO_2. The lighter effective mass and longer lifetime of the excess electrons in the anatase TiO_2 spheres enable a slower recombination rate between the electrons and holes than is the case with rutile TiO_2.

Funding

The Basic Science Research Program of the National Research Foundation of Korea (NRF), funded by the Ministry of Education, Science and Technology (NRF-2015R1A1A1A05027848)